KINETIC GAS DISKS SURROUNDING SCHWARZSCHILD BLACK HOLES*

Carlos Gabarrete, Olivier Sarbach

Instituto de Física y Matemáticas
Universidad Michoacana de San Nicolás de Hidalgo
Edificio C-3, Ciudad Universitaria, 58040 Morelia, Michoacán, México

Received 1 December 2021, accepted 3 December 2021, published online 31 January 2022

We describe stationary and axisymmetric gas configurations surrounding black holes. They consist of a collisionless relativistic kinetic gas of identical massive particles following bound orbits in a Schwarzschild exterior spacetime and are modeled by a one-particle distribution function which is the product of a function of the energy and a function of the orbital inclination associated with the particle's trajectory. The morphology of the resulting configuration is analyzed.

DOI:10.5506/APhysPolBSupp.15.1-A10

1. Introduction

In recent years, there has been interest in analyzing the properties of solutions to the Vlasov equation on a fixed, curved background spacetime. In particular, such an analysis has been performed for a Schwarzschild background with the aim of understanding the Bondi–Michel and Bondi–Hoyle–Littleton accretion models for a collisionless kinetic gas [1–3]. Also, kinetic analogues of the perfect fluid "Polish doughnuts" configurations are discussed in [4]. Similarly to their fluid counterparts, they describe stationary and axisymmetric disks around black holes, where the individual gas particles follow bound timelike geodesics in a Schwarzschild spacetime. In [4], these configurations are modeled by a one-particle distribution function (DF) depending only on the energy E, azimuthal L_z, and total angular momentum L of the particles. Examples are given in which the DF is described by a generalized polytropic ansatz [5, 6] depending only on E and L_z. In this article, we provide additional examples where the DF is a function of E and

* Presented at the 7$^{\text{th}}$ Conference of the Polish Society on Relativity, Łódź, Poland, 20–23 September 2021.

the inclination angle i defined by $\cos i = L_z/L$. We analyze the behavior of the resulting particle density and compute the total number of particles of the gas cloud as a function of the free parameters in our ansatz.

2. The model

We work in the Schwarzschild exterior spacetime, written in the usual coordinates $(t, r, \vartheta, \varphi)$, with metric[1]

$$g := -N(r)\mathrm{d}t^2 + \frac{\mathrm{d}r^2}{N(r)} + r^2\left(\mathrm{d}\vartheta^2 + \sin^2\vartheta \mathrm{d}\varphi^2\right), \qquad N(r) := 1 - \frac{2M}{r} > 0, \tag{1}$$

where $M > 0$ is the mass of the black hole. Since this spacetime is static and spherically symmetric, the particle's rest mass m is conserved along with E, L, and L_z. In terms of the orthonormal tetrad $e_{\hat{0}} = N(r)^{-1/2}\partial_t$, $e_{\hat{1}} = N(r)^{1/2}\partial_r$, $e_{\hat{2}} = r^{-1}\partial_\vartheta$, $e_{\hat{3}} = (r\sin\vartheta)^{-1}\partial_\varphi$, the four-momentum of the particles can be parametrized as $p = p^{\hat{\mu}}e_{\hat{\mu}}$ with (see [2, Eq. (58)])

$$\left(p^{\hat{\mu}}\right) = \left(\frac{E}{\sqrt{N(r)}}, \epsilon_r\sqrt{\frac{E^2 - V_L(r)}{N(r)}}, \frac{\epsilon_\vartheta}{r}\sqrt{L^2 - \frac{L_z^2}{\sin^2\vartheta}}, \frac{L_z}{r\sin\vartheta}\right), \tag{2}$$

where the signs $\epsilon_r = \pm 1$ and $\epsilon_\vartheta = \pm 1$ determine the direction of motion in the radial and polar directions, respectively, and $V_L(r) = N(r)(m^2 + L^2/r^2)$ is the effective potential for the radial motion.

A collisionless relativistic gas consisting of identical massive particles of mass m trapped in V_L is described by a DF which relaxes in time to a DF depending only on integrals of motion. This is due to phase mixing, see *e.g.* [7, 8] and references therein. Here, we assume, in addition, that the final configuration is axisymmetric, which implies that the DF has the form of

$$f(x, p) = F(E, L, L_z) \tag{3}$$

for some function F which we shall specify shortly. The relevant spacetime observables are the particle current density vector field J and the energy-momentum-stress tensor T defined by

$$J_{\hat{\mu}}(x) := \int_{P_x^+(m)} f(x,p)p_{\hat{\mu}}\mathrm{dvol}_x(p), \qquad T_{\hat{\mu}\hat{\nu}}(x) := \int_{P_x^+(m)} f(x,p)p_{\hat{\mu}}p_{\hat{\nu}}\mathrm{dvol}_x(p), \tag{4}$$

where $\mathrm{dvol}_x(p) = \mathrm{d}p^{\hat{1}} \wedge \mathrm{d}p^{\hat{2}} \wedge \mathrm{d}p^{\hat{3}}/p^{\hat{0}}$ is the Lorentz-invariant volume form on the future mass hyperboloid $P_x^+(m)$ of mass m at x, see [9] for details.

[1] We use units in which the speed of light and the gravitational constant are one.

For the following, we focus on the particular ansatz

$$F(E, L, L_z) := F_0(E) \cos^{2s}(i)\,, \qquad F_0(E) = \alpha \left(1 - \frac{E}{m}\right)_+^{k-\frac{3}{2}}\,, \tag{5}$$

where $\alpha > 0$, $k > 1/2$ are constants, i is the inclination angle, and $s \geq 0$ is a parameter. The notation f_+ refers to the positive part of the quantity f, that is $f_+ = f$ if $f > 0$ and $f_+ = 0$ otherwise. Here, the function F_0 is the general relativistic generalization of the polytropic ansatz [10], while the parameter s controls the concentration of the orbits near the equatorial plane $\vartheta = \pi/2$ (see Fig. 1).

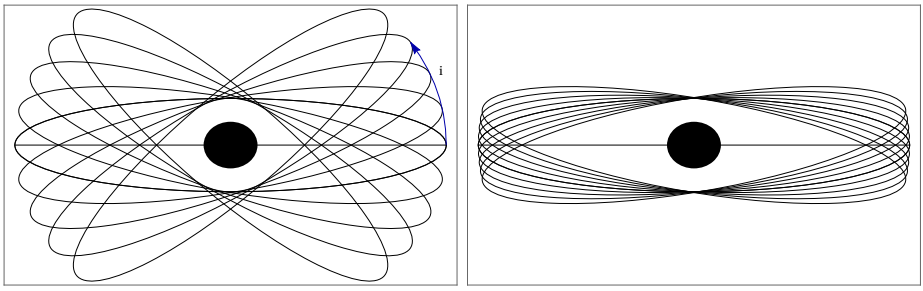


Fig. 1. Illustration of the effect of the parameter s (left panel for small s, right panel for large s). As s increases, orbits confined to planes lying close to the equatorial one become more populated, such that the configuration becomes a thin disk in the limit $s \to \infty$.

For the following, we introduce the dimensionless quantities $\xi := r/M$, $\lambda := L/(Mm)$, $\varepsilon := E/m$, and $U_\lambda(\xi) := V_L(r)/m^2$, and parametrize the future mass hyperboloid $P_x^+(m)$ in terms of the quantities $(\varepsilon, \lambda, \chi)$, where the angle χ is defined by $(p^{\hat{2}}, p^{\hat{3}}) = \frac{m\lambda}{\xi}(\cos\chi, \sin\chi)$ which implies $\cos i = \sin\vartheta \sin\chi$. For bound orbits, these quantities are restricted to the following domain (see [11, Appendix A] and [4, Appendix A]):

$$\varepsilon_{\rm c}(\xi) < \varepsilon < 1\,, \qquad \lambda_{\rm c}(\varepsilon) \leq \lambda \leq \lambda_{\max}(\varepsilon, \xi)\,, \quad \text{and} \qquad 0 \leq \chi \leq 2\pi\,, \tag{6}$$

where $\varepsilon_{\rm c}(\xi)$ is the minimum energy at radius ξ, $\lambda_{\rm c}(\varepsilon)$ is the critical value for the total angular momentum for which the maximum of the potential barrier in $U_\lambda(\xi)$ is exactly equal to ε^2, and $\lambda_{\max}(\varepsilon, \xi)$ is the maximum angular momentum permitted at the energy ε and radius ξ. Note that the domain (6) is empty if $\xi < 4$, since for a Schwarzschild black hole, the minimum radius for bound orbits is $r = 4M$.

For the ansatz (5), the fibre integrals in Eq. (4) yield

$$J_{\hat{\mu}}(x) = \frac{m^2 \sin^{2s}\vartheta}{\xi^2} \sum_{\epsilon_r=\pm 1} \int_{\varepsilon_{\rm c}(\xi)}^{1} \int_{\lambda_{\rm c}(\varepsilon)}^{\lambda_{\max}(\varepsilon,\xi)} \int_0^{2\pi} p_{\hat{\mu}} F_0(E) \sin^{2s}\chi \frac{{\rm d}\varepsilon\, \lambda\, {\rm d}\lambda\, {\rm d}\chi}{\sqrt{\varepsilon^2 - U_\lambda(\xi)}}\,, \quad (7)$$

and similarly for $T_{\hat{\mu}\hat{\nu}}(x)$. Using expressions (2) for the four-momentum, the non-vanishing orthonormal components of $J^{\hat{\mu}}$ and $T^{\hat{\mu}}{}_{\hat{\nu}}$ are

$$J^{\hat{0}} = 4\sqrt{\pi}\frac{\sin^{2s}\vartheta}{N^{3/2}}\frac{\Gamma(s+1/2)}{\Gamma(s+1)} m^3 \int_{\varepsilon_{\rm c}(\xi)}^{1} {\rm d}\varepsilon\varepsilon Y(\varepsilon,\xi)^{1/2} F_0(m\varepsilon)\,, \quad (8)$$

$$T^{\hat{0}}{}_{\hat{0}} = -4\sqrt{\pi}\frac{\sin^{2s}\vartheta}{N^2}\frac{\Gamma(s+1/2)}{\Gamma(s+1)} m^4 \int_{\varepsilon_{\rm c}(\xi)}^{1} {\rm d}\varepsilon\varepsilon^2 Y(\varepsilon,\xi)^{1/2} F_0(m\varepsilon)\,, \quad (9)$$

$$T^{\hat{1}}{}_{\hat{1}} = \frac{4\sqrt{\pi}}{3}\frac{\sin^{2s}\vartheta}{N^2}\frac{\Gamma(s+1/2)}{\Gamma(s+1)} m^4 \int_{\varepsilon_{\rm c}(\xi)}^{1} {\rm d}\varepsilon Y(\varepsilon,\xi)^{3/2} F_0(m\varepsilon)\,, \quad (10)$$

$$T^{\hat{2}}{}_{\hat{2}} = \frac{4\sqrt{\pi}}{3}\frac{\sin^{2s}\vartheta}{N^2}\frac{\Gamma(s+1/2)}{\Gamma(s+2)} m^4 \int_{\varepsilon_{\rm c}(\xi)}^{1} {\rm d}\varepsilon Y(\varepsilon,\xi)^{1/2} Z(\varepsilon,\xi) F_0(m\varepsilon)\,, \quad (11)$$

$$T^{\hat{3}}{}_{\hat{3}} = (2s+1) T^{\hat{2}}{}_{\hat{2}}\,, \quad (12)$$

where we have introduced the shorthand notation

$$Y(\varepsilon,\xi) := \varepsilon^2 - N(r)\left[1 + \frac{\lambda_{\rm c}(\varepsilon)^2}{\xi^2}\right], \qquad Z(\varepsilon,\xi) := \varepsilon^2 - N(r)\left[1 - \frac{\lambda_{\rm c}(\varepsilon)^2}{2\xi^2}\right]. \quad (13)$$

The quantities (8)–(12) determine the relevant macroscopic observables, namely the particle density $n = J^{\hat{0}}$, energy density $\mathcal{E} = -T^{\hat{0}}{}_{\hat{0}}$, and the principal pressures $P_1 = T^{\hat{1}}{}_{\hat{1}}$, $P_2 = T^{\hat{2}}{}_{\hat{2}}$, and $P_3 = (2s+1)P_2$. Note that all of these quantities have the dependency of $\sin^{2s}\vartheta$ with respect to the polar angle ϑ. In the limit $s = 0$, the configurations describe a spherical shell of gas trapped in the region of $\xi > 4$, while for $s = 1/2, 1, 3/2, \ldots$, they are axisymmetric, the macroscopic variables being zero for $\xi \leq 4$ and along the axis $\vartheta = 0, \pi$. In the next section, we analyze the morphology of these configurations as a function of the parameters k and s for a fixed total particle number.

3. Total particle number and behavior of the particle density

The (conserved) total particle number $\mathcal{N}$ is defined as minus the flux integral of the current density vector field with respect to a Cauchy surface. This in turn can be rewritten as an integral over the six-dimensional phase space parametrized by (x^i, p_i). To compute this integral, it is convenient to transform (x^i, p_i) to action-angle variables $(\mathcal{Q}^i, \mathcal{J}_i)$. The integral over the angle variables $\mathcal{Q}^i$ yields a factor $(2\pi)^3$, while the integral over the action variables can be rewritten in terms of the conserved quantities (E, L, L_z), taking into account that $\mathrm{d}^3\mathcal{J} = T(E,L)\mathrm{d}E\,\mathrm{d}L\,\mathrm{d}L_z/2\pi$, where $T(E,L)$ is the period function for the radial motion. For the Schwarzschild spacetime, this function can be expressed in terms of elliptic integrals and has the form of $T(E,L) = 2M\varepsilon\,[\mathbb{H}_2 - \mathbb{H}_0]$ (see [7, Appendix A] and [4] for the explicit form of $\mathbb{H}_2$ and $\mathbb{H}_0$ in the Schwarzschild case). For ansatz (5), this yields the following expression for the total particle number:

$$\mathcal{N} = \frac{16\pi^2}{2s+1}(Mm)^3\alpha \int_{\varepsilon_{\min}}^{1} \mathrm{d}\varepsilon\, \varepsilon\,(1-\varepsilon)_+^{k-\frac{3}{2}} \int_{\lambda_c(\varepsilon)}^{\lambda_{\mathrm{ub}}(\varepsilon)} \mathrm{d}\lambda\, \lambda\,(\mathbb{H}_2 - \mathbb{H}_0)\,, \qquad (14)$$

where $\varepsilon_{\min} = \sqrt{8/9}$ and $\lambda_{\mathrm{ub}}(\varepsilon)$ is given in [11, Appendix A]. To compute this integral, it is convenient to re-parametrize the orbits in terms of their eccentricity e and "semi-latus rectum" P, related to the turning points (ξ_1, ξ_2) by $\xi_1 = P/(1+e)$ and $\xi_2 = P/(1-e)$, and to the conserved quantities (ε, λ) according to [4, 7, 12, 13] $(\varepsilon^2, \lambda^2) = (P^{-1}[(P-2)^2 - 4e^2], P^2)/(P - e^2 - 3)$. Here, (P, e) are restricted to the domain $0 < e < 1$ and $P > 6 + 2e$. The resulting integral is then calculated numerically using Mathematica. The total mass is simply $m\mathcal{N}$ and the total energy is given by the same expression as in Eq. (14) with an extra factor $m\varepsilon$ inside the integral.

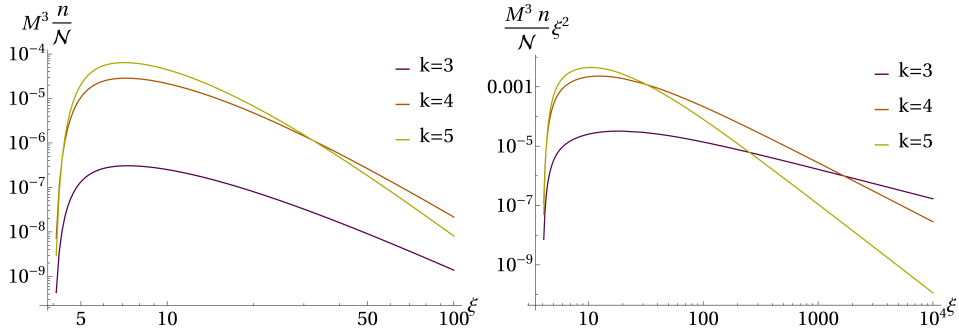


Fig. 2. Left panel: Dimensionless profile of the particle density in the equatorial plane for $k = 3, 4, 5$ and $s = 1$ in a logarithmic scale. Right panel: The same quantity multiplied with ξ^2 which shows that even though configurations with higher values of k have a larger maximum, they have a faster decay at infinity.

In Fig. 2, we show the dimensionless quantity $M^3 n/\mathcal{N}$ in the equatorial plane for several values of k and $s = 1$. In Fig. 3, we show contour plots of the same quantity in the xz-plane for $k = 3$ and two different values of s.

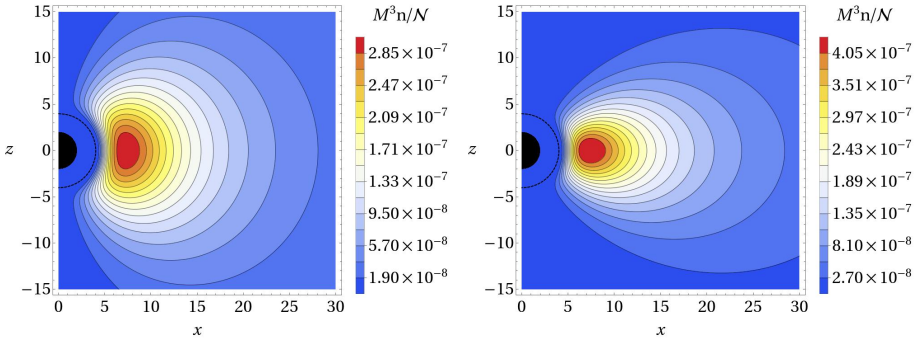


Fig. 3. Contour plots for the particle density in the xz-plane for the configurations with $k = 3$ and $s = 1$ (left panel) and $k = 3$ and $s = 3$ (right panel). Here, $(x, z) = r(\sin\vartheta, \cos\vartheta)$, the black region represents the black hole interior and the dashed black circles the interior boundary of the disk. As it is visible from these plots, the configuration with higher s yields a thinner disk.

4. Conclusions

We described a family of stationary and axisymmetric collisionless gas configurations which are trapped in the gravitational potential of a Schwarzschild black hole. This family depends on two parameters s and k which control the thickness of the disk and its radial density distribution. An alternative model is discussed in detail in [4]. We expect these configurations to serve as a first approximation for the description of low-luminosity disks surrounding black holes.

We acknowledge support from a CIC grant to Universidad Michoacana and CONACyT Frontier Project No. 376127.

REFERENCES

[1] P. Rioseco, O. Sarbach, «Spherical steady-state accretion of a relativistic collisionless gas into a Schwarzschild black hole», *J. Phys. Conf. Ser.* **831**, 012009 (2017).

[2] A. Gamboa *et al.*, «Accretion of a Vlasov gas onto a black hole from a sphere of finite radius and the role of angular momentum», *Phys. Rev. D* **104**, 083001 (2021).

[3] P. Mach, A. Odrzywołek, «Accretion of Dark Matter onto a Moving Schwarzschild Black Hole: An Exact Solution», *Phys. Rev. Lett.* **126**, 101104 (2021).

[4] C. Gabarrete, O. Sarbach, «Axisymmetric, stationary collisionless gas configurations surrounding black holes», in preparation, 2022.

[5] E. Ames, H. Andréasson, A. Logg, «On Axisymmetric and Stationary Solutions of the Self-Gravitating Vlasov System», *Class. Quantum Grav.* **33**, 155008 (2016).

[6] E. Ames, H. Andréasson, A. Logg, «Cosmic String and Black Hole Limits of Toroidal Vlasov Bodies in General Relativity», *Phys. Rev. D* **99**, 024012 (2019).

[7] P. Rioseco, O. Sarbach, «Phase space mixing in the equatorial plane of a Kerr black hole», *Phys. Rev. D* **98**, 124024 (2018).

[8] P. Rioseco, O. Sarbach, «Phase space mixing in an external gravitational central potential», *Class. Quantum Grav.* **37**, 195027 (2020).

[9] R. Acuña-Cárdenas, C. Gabarrete, O. Sarbach, «An introduction to the relativistic kinetic theory on curved spacetimes», arXiv:2106.09235 [gr-qc].

[10] J. Binney, S. Tremaine, «Galactic Dynamics», *Princeton University Press*, Princeton, New Jersey 2008.

[11] P. Rioseco, O. Sarbach, «Accretion of a relativistic, collisionless kinetic gas into a Schwarzschild black hole», *Class. Quantum Grav.* **34**, 095007 (2017).

[12] W. Schmidt, «Celestial mechanics in Kerr spacetime», *Class. Quantum Grav.* **19**, 2743 (2002).

[13] J. Brink, M. Geyer, T. Hinderer, «Astrophysics of resonant orbits in the Kerr metric», *Phys. Rev. D* **91**, 083001 (2015).